Fabrication, characterization, and biological properties evaluation of bioactive scaffold based on mineralized carbon nanofibers

Mehdi Azizi[1], Amin Shavandi[2], Masoud Hamidi[2,3], Shayan Gholizadeh[4], Mahnaz Mohammadpour[5], Mohammad Saeid Salami[6], Hadi Samadian[7*]

1. Dental Implants Research Center, Hamadan University of Medical Sciences, Hamadan, Iran
2. BioMatter-Biomass Transformation Lab (BTL), École Polytechnique de Bruxelles, Université Libre de Bruxelles,
3. Department of Medical Biotechnology, Faculty of Paramedicine, Guilan University of Medical Sciences, Rasht, Iran
4. Department of Biomedical Engineering, Rochester Institute of Technology, Rochester, NY, USA
5. Department of Chemistry, Faculty of Sciences, Tarbiat Modares University, Tehran, Iran
6. Nano Drug Delivery Research Center, Health Technology Institute, Kermanshah University of Medical Sciences, Kermanshah, Iran
7. Research Center for Molecular Medicine, Hamadan University of Medical Sciences, Hamadan, Iran

Correspondence address

Hadi Samadian, Email: h30samadiyan@gmail.com

ORCID: https://orcid.org/**0000-0002-2478-5709**

Abstract

Tissue engineering as an innovative approach aims to combine engineering, biomaterials, and biomedicine to eliminate the drawbacks of conventional bone defect treatment. In the current study, we fabricated bioengineered electroactive and bioactive mineralized carbon nanofibers as the scaffold for bone tissue engineering applications. The scaffold was fabricated using the sol-gel method and thoroughly characterized by SEM imaging, EDX analysis, and a 4-point probe. The results showed that the CNFs have a diameter of 200 ± 19 nm and electrical conductivity of 1.02 ± 0.12 $S.cm^{-1}$. The in vitro studies revealed that the synthesized CNFs were osteoactive and supported the mineral crystal deposition. The hemolysis study confirmed the hemocompatibility of the CNFs and cell viability/proliferation sassy using an MTT assay kit showed the proliferative activities of mineralized CNFs. In conclusion, this study revealed that the mineralized CNFs synthesized by the combination of sol-gel and electrospinning techniques were electroactive, osteoactive, and biocompatible, which can be considered an effective bone tissue engineering scaffold.

Keywords: Bone regeneration; Tissue engineering; Carbon nanofibers; Electroconductive; Bioactive

1. Introduction

Bone is a natural composite of collagen nanofibers and hydroxyapatite crystals with a wide range of functions in the body. It has the potential to repair minor defects in normal situations, while in large defects and abnormal conditions, the healing process goes not properly and required some interventions [1-3]. Autografts are the gold standard treatment for large bone defects. Despite their positive outcomes, they suffer from some substantial issues, such as graft resorption, donor site morbidity, need for a second surgery, and restricted bone availability [4, 5]. The tissue engineering concept has emerged to eliminate the limitations of the current treatment and provide more effective treatment. Tissue engineering is a multidisciplinary approach, combining scaffolds, cells, and bioactive molecules to treat and maintain anatomical and functional tissue damages [6, 7]. Scaffolds play central roles in this scenario and act not only as a support to guide cell growth and migration but also as a vehicle to deliver the therapeutic agents locally. Accordingly, unprecedented attention has been devoted to the design, fabrication, modification, characterization, and application of various forms of scaffolds for bone regeneration applications [8, 9].

The similarity of the fabricated scaffolds to the native structure of bone in the forms of architecture, mechanical, and physicochemical properties, along with the biocompatibility and non-immunogenicity, are vital requirements for an effective and successful bone tissue engineering scenario [10]. Collagen nanofibers have determinant roles in the extracellular matrix (ECM) of bone, and nanofibrous scaffolds can mimic these features. Nanofibers have shown fascinating properties beneficial for tissue engineering applications, such as ECM resemblance, high surface-to-volume ratio, tunable porosity, and loading capacity for different drugs/bioactive molecules [11, 12]. Electrospinning is a sophisticated method of nanofibers fabrication with various promising specifications, such as simplicity, flexibility to use different natural and synthetic polymers, and fabrication of nanofibers with different morphology and

architecture. Plenty of studies have reported the application of electrospun nanofibers as the scaffold for bone tissue engineering [13, 14]. Mineralized scaffolds have shown promising results in bone regeneration due to their similarity to bone tissue. Different approaches have been reported for fabricating mineralized scaffolds, such as the incorporation of bioceramics (*e.g.,* hydroxyl apatite, bioglass, β-TCP crystals), biomimetic mineralization in simulated body fluid (SBF), and the sol-gel method. Each method has its weakness and strength. The sol-gel method is a well-established and sophisticated method for fabricating various nanostructures and tissue engineering scaffolds [15, 16].

It has been shown that bone is an electroactive tissue, and there are electrical signals and charge transfer in bone tissue, which can modulate bone formation and density. Various studies have revealed positive effects of electrical stimulation on bone cell proliferation, migration, and differentiation [17-19]. Using electroconductive scaffolds/substrates is a practical approach to precisely delivering the electrical signal to the bone defect site. Moreover, the application of electroconductive scaffolds can transfer and guide the generated electrical signals to the defect site and affect the healing involved cells [20-23]. Accordingly, many studies have been conducted on developing electroconductive scaffolds for bone tissue engineering. Carbon-based nanostructures have exhibited fascinating properties applicable in medicine [24-26]. Carbon nanostructures are among the most widely used nanomaterials used in medicine. The wide range application of carbon nanostructures can be related to availability of different allotropes of carbon, inimitable features, well-established chemistry, and their nanometric size [27-29]. Carbon nanofibers (CNFs) are interesting structures due to their unique mechanical strength, electrical conductivity, chemical inertness, and biocompatibility. Combining CNFs with the sol-gel mineralization approach can result in a bioactive and electroactive scaffold for bone regeneration. In a tissue engineering strategy, it is critical to fabricate a scaffold that mimics the structure of native tissue as much as possible. Accordingly, we fabricated

nanofibrous, electroconductive, and bioactive scaffolds tailored for bone tissue engineering in the current study. The combination of the carbonization electrospun precursor polymeric nanofibers with the well-established sol-gel synthesis method is the novelty of the current work, which has been less discussed in previous studies.

2. Materials and methods

2.1. Chemicals

PAN (average Mw 150,000), Triethyl phosphate (TEP), Calcium nitrate tetrahydrate (CN), tetraethoxysilane (TEOS), NaCl, $NaHCO_3$, Na2SO4, KCl, $K_2HPO_4 \cdot 3H_2O$, $MgCl_2 \cdot 6H_2O$, $CaCl_2 \cdot 2H_2O$, 4′,6-Diamidine-2′-phenylindole dihydrochloride (DAPI), and Paraformaldehyde (PFA) were purchased from Sigma-Aldrich (St. LouisMO, USA). FBS (Fetal Bovine Serum), DMEM/F-12 cell culture medium, Pen-Strep (Penicillin-Streptomycin) and Trypsin-EDTA were obtained from Gibco (Germany). MTT assay kit was purchased from Roth (Germany).

2.2. Mineralized CNFs fabrication

The mineralized CNFs were fabricated using the sol-gel method with some modifications [30, 31]. The sol-gel solution was prepared by dissolving TEP in a mixture of DI water and absolute alcohol and stirred at 80 °C for 24 to hydrolyze TEP. Then, CN and TEOS were added to the hydrolyzed TEP solution and stirred for 120 at room temperature. The prepared sol-gel solution was added dropwise to PAN/DMF solution (10 wt.%) and stirred for 24 h at 40°C. The prepared solution was electrospun using a commercial electrospinning apparatus with the feeding rate, applied voltage, and nozzle to collector distance of 1 ml/min, 20 kV, and 10 cm, respectively. The fabricated nanofibers were hydrolyzed at 50 °C for 24 h and carbonized by two steps heat treatment, stabilization at 280 °C for two h and carbonization at 1000 °C for one h in an N2 atmosphere.

2.3. Characterization

2.3.1. Nanofibers morphology

The morphology of the prepared nanofibers was observed using scanning electron microscopy (SEM, FEI, quanta 450, USA) at 20 kV accelerating voltage after sputter coating with a thin layer of gold using a sputter coater (SCD 004, Balzers, Germany). The diameter of nanofibers was calculated using Image J software (1.47v, National Institute of Health, USA). EDX detector-equipped SEM system was used to conduct semi-quantitative elemental analysis on nanofibers.

2.3.2. Electrical conductivity measurement

The electrical conductivity of the prepared nanocomposite was measured by the standard four points probe multi-meter (Signatone SYS-301 with Keithley196 system DDM multimeter).

2.4. Bioactivity assessment

The prepared nanocomposites' bioactivity (also known as osteocompatibility) was assessed through their biomineralization in simulated body fluid (SBF). The SPB solution was prepared by dissolving various reagent-grade salts, such as Na_2SO_4, NaCl, $K_2HPO_4{\cdot}3H_2O$, $NaHCO_3$, KCl, $CaCl_2{\cdot}2H_2O$, and $MgCl_2{\cdot}6H_2O$ in distilled water and buffering at pH: 7.4 with Tris–HCl at 37 ± 0.2 °C. The pristine and sole-gel CNFs mats (1 × 2 cm) were incubated in the prepared SBF under continuous shaking for 7 and 14 days at 37 °C. The CNFs were removed from the SBF solution, washed with distilled water, and evaluated using SEM imaging and EDX analysis.

2.5. **Hemocompatibility analysis**

Hemolysis induced by the fabricated CNFs was measured as the hemocompatibility induction of the nanofibers. Fresh anti-coagulated blood was diluted with PBS (2:2.5 mL) and 200 µL of the diluted blood was incubated with 100 mg of CNFs at 37°C for one h. Then, the samples were centrifuged for 10 min at 1500 rpm and the supernatants were transferred to a 96-wells

plate and their absorbance read at 545 nm using the Microplate Reader. Equation 1 was used to calculate the hemolysis percent [32].

$$\text{Hemolysis (\%)} = \frac{Dt-Dnc}{Dpc-Dnc} \times 100 \quad \text{Eq. 1}$$

2.6. Cell toxicity investigation

The toxicity of the prepared nanocomposites on MG-63 cells was measured using the lactate dehydrogenase (LDH) assay kit [33]. The nanocomposites were cut circulatory and put at the bottom of the well of 96-wells palate, sterilized using UV irradiation and ethanol 70%. The sterilized nanofibers were washed with sterilized PBS three times and incubated for two h with DMEM cell culture medium supplemented with FBS (10% v/v) and Pen/Strep (100 unit/mL and 100 µg/mL). Then, a number of 5,000 cells suspended in a 100 µL DMEM cell culture medium supplemented with FBS (1.0% v/v) and Pen/Strep was seeded on the CNFs and incubated a humidified cell culture incubator at 37 °C with CO_2 (5%) for 24 and 72 h. After passing the incubation times, the toxicity was evaluated based on the procedure described by the manufacturer and Equation (2) [33].

$$\text{Cytotoxicity (\%)} = \left(\frac{\text{exp.value} - \text{low control}}{\text{high control} - \text{low control}}\right) \times 100 \quad \text{Eq. 2}$$

2.7. Cell attachment and morphology observation

The attachment and morphology of MG-63 cells on the prepared nanocomposites were evaluated using DAPI staining and SEM imaging, respectively. For the DPI staining, the CNFs were sterilized and prepared based on the previous section, and a number of 3,000 cells suspended in 100 µL DMEM cell culture medium supplemented with FBS (10% v/v) and Pen/Strep was seeded on the CNFs and incubated a humidified cell culture incubator at 37 °C with CO2 (5%) for 72 h. After passing the time point, the cell culture was aspirated, and the

cells were washed three times with sterilized PBS and incubated with PFA 4% in PBS for 60 min at 4 °C to fix the cells. In the next step, PFA was aspirated and the cells were washed with PBS several times and incubated with 60 µL of triton x100 for 10 min to permeable the cell's membrane for DPI stain. Finally, the cells were incubated with 50 µL DAPI stain diluted in PBS (1: 1,000) and the cells were observed under fluorescent microscopy.

The morphology of MG-63 cells on the prepared CNFs was evaluated using SEM imaging. The CNFs were sterilized based on the previous experiment and a number of 5,000 cells were seeded on CNFs and incubated in a cell culture incubator at 37 °C with CO2 (5%) for 24 h. After passing the incubation time, the cells were washed three times with PBS, fixed with PFA 4% in PBS for 60 min at 4 °C, and dehydrated in graduated ethanol. The fixed cells were sputter-coated with a thin layer of gold and observed at 20.0 kV accelerating voltage.

1.1. Statistical analysis

The statistical analysis was conducted using the SPSS program v.23 (IBM, Armonk, NY, USA) by applying the one-way analysis of variance (ANOVA) and Tukey's multiple comparison test ($p < 0.05$). All tests were performed in triplicate except the hemocompatibility and cytocompatibility conducted on five samples in each group.

2. Results and discussion

2.1. Nanofibers morphology and Elemental analysis results

The morphology of the prepared nanofibers (PAN, CNFs, and nanocomposite) was observed using SEM imaging and the results are presented in Fig. 1. The results showed that the prepared PAN nanofibers were straight, uniform, and beadless (Fig. 1a). On the other hand, some fusions and integrations between nanofibers are observed in the CNFs derived from the PAN nanofibers (Fig. 1b). These fusions and structural deformations can be attributed to the

interactions between PAN polymer chains with oxygen molecules during the stabilization process (at 280 °C in the air), which is critical to preserve nanofibers' integrity and structure during the carbonization process [34]. The mineralization of nanofibers and the formation of mineral crystals on nanofibers are apparent in Fig. 1 c and d. Moreover, The EDX analysis confirmed the presence of calcium crystals in the nanofibrous composite after the calcination process (Fig. 1 e and f).

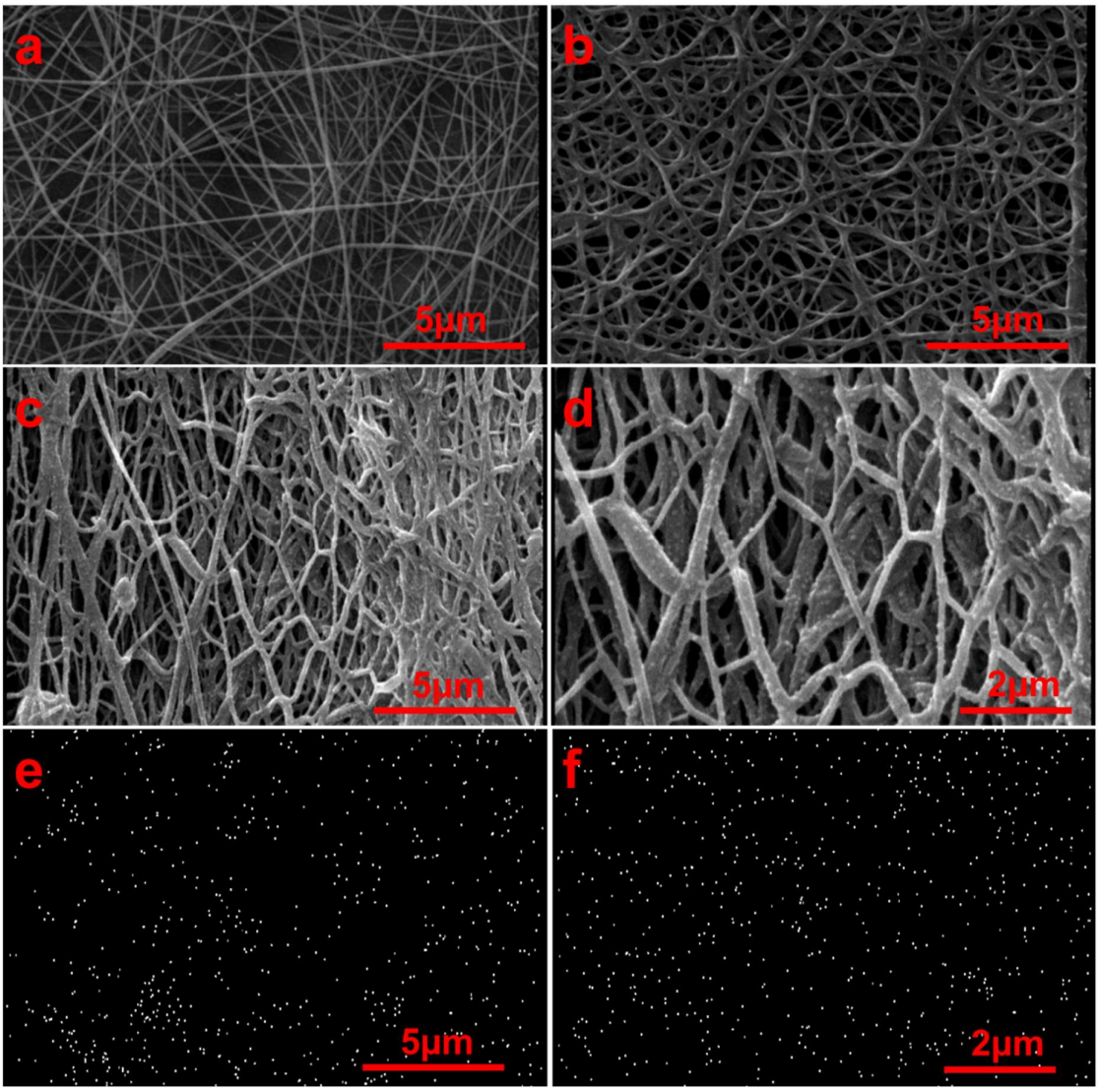

Fig. 1. SEM micrograph of the nanofibers and EDX analysis of the nanocompostie. (a) SEM image of PAN nanofibrs, (b) SEM image of pristine CNFs, (c) low magnified SEM image of mirealized CNFs, (d) high magnified SEM image of mineralized CNFs, (e) and (f) EDX elemental analysis of mineralized CNFs.

The diameter of nanofibers was measured using ImageJ software based on the SEM images. The results showed that the PAN nanofiber's diameter was 148 ± 27 nm, and the carbonization reduced the diameter to 125 ± 20 nm, which can be attributed to the partial shrinkage of nanofibers and the removal of non-carbonaceous substances. Mirzaei et al. [35] fabricated PAN-derived CNFs as the scaffold for neural tissue engineering and reported some structural deformations and dimeter reduction after carbonization of PAN nanofibers. In another study, Yang et al. [30] applied the sol-gel method to fabricate mineralized CNFs as the bone regenerating structure and observed the formation of calcium/phosphate crystals on the CNFs.

2.2. Electrical conductivity values

The electrical conductivity of the scaffold has an essential role in bone regeneration. Accordingly, we measured the electrical conductivity of the prepared nanocomposite using the 4-point probe device. The results showed that the electrical conductivity of pristine and mineralized CNFs was 2.45 ± 0.03 $S.cm^{-1}$ and reduced to 1.12 ± .025 $S.cm^{-1}$, respectively. The observed reduction in electrical conductivity of mineralized CNFs compared with the pristine CNFs can be related to the formation of calcium/phosphate crystals within the CNFs, which compromised the electrical conductivity. Compared with the other similar structure (carbon nanotubes, CNTs), CNFs exhibit lower crystallinity and more amorphous microstructure, more electrical resistance and lower conductivity, poor mechanical properties, and smaller surface areas, but, CNFs have been shown to offer more biocompatibility, lower fabrication costs, and better dispersion in aqueous media [36, 37].

Zhou et al. [38] CNFs derived from PAN nanofibers have suitable electrical conductivity. Moreover, they observed that the electrical conductivity significantly depends on the direction of electrical conductivity measurement. Such that, measurement in the parallel direction of CNFs alignment showed 20 times higher than in the perpendicular direction. Moreover, they reported that the carbonization temperature substantially affects the electrical conductivity and higher carbonization temperature results in a higher electrical conductivity due to the formation of more graphitic and ordered structures.

2.3. Wettability results

The wettability of scaffolds is a critical property determining the fate of scaffolds within the body since it affects the surface adsorption of proteins and biomolecules. It has been shown that the proteins of biological fluids adsorb more extensively on the hydrophobic compared with the hydrophilic surface. During the protein adsorption process, some structural changes and deformations may induce, which activates the foreign body reaction. The activation of immune response may finality result in scaffold failure. The wettability of the prepared scaffolds was measured using the water contact angle (WCA) method and the results are presented in Fig. 2. The results showed that the fabricated pristine CNFs were hydrophobic with the WCA value of 117 ± 5˚, while the mineralized CNFs were hydrophilic with the WCA value of 53 ± 5˚. The observed hydrophilicity is related to the formation of mineral crystals on CNFs.

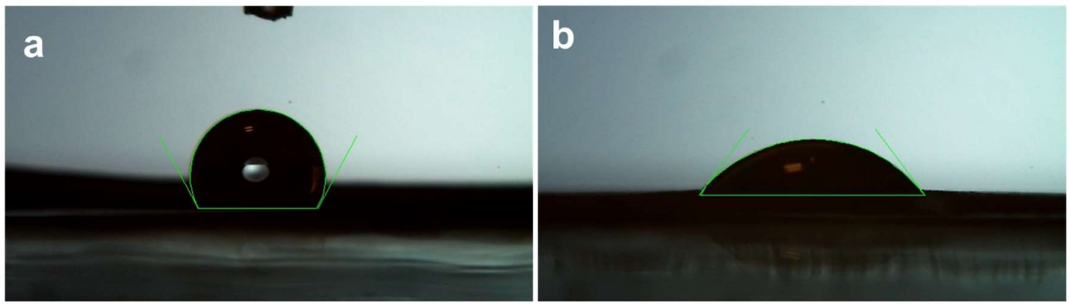

Fig. 2. Wettability of the prepared (a) pristine CNFs and (b) mineralized CNFs evaluated by the water contact angle value.

2.4. Bioactivity findings

The bioactivity of the prepared nanocomposites was measured in SBF solution to assess the calcium/phosphate crystal formation on the nanofibers. This ability to support calcium/phosphate crystal formation on the scaffolds is also termed osteoactivity. The results showed that the calcium/phosphate crystals were formatted heterogeneously on the pristine CNFs. The crystals formed on the outer layer of nanofibers, and there are no crystals on the deepest part of pristine CNFs. These crystals' formation pattern is related to the hydrophobic nature of the pristine CNFs, which do not allow the diffusion of SBF solution to the deep of CNFs.

On the other hand, the calcium/phosphate crystals were formatted heterogeneously on the mineralized CNFs. Moreover, the diffusion of SBF solution into the deep of the mineralized CNFs and crystal formation in this region is apparent. This crystals formation pattern is also due to the hydrophilic nature of mineralized CNFs, which allow the diffusion of the solution to the deep layer of nanofibrous mat. Wu et al. [39] fabricated PAN-derived CNFs. They observed that the hydrophobic nature of CNFs did not allow hydroxyapatite crystals formation in the deep of the mate. At the same time, NaOH treatment resulted in surface hydrophilicity and crystal formation throughout the mat.

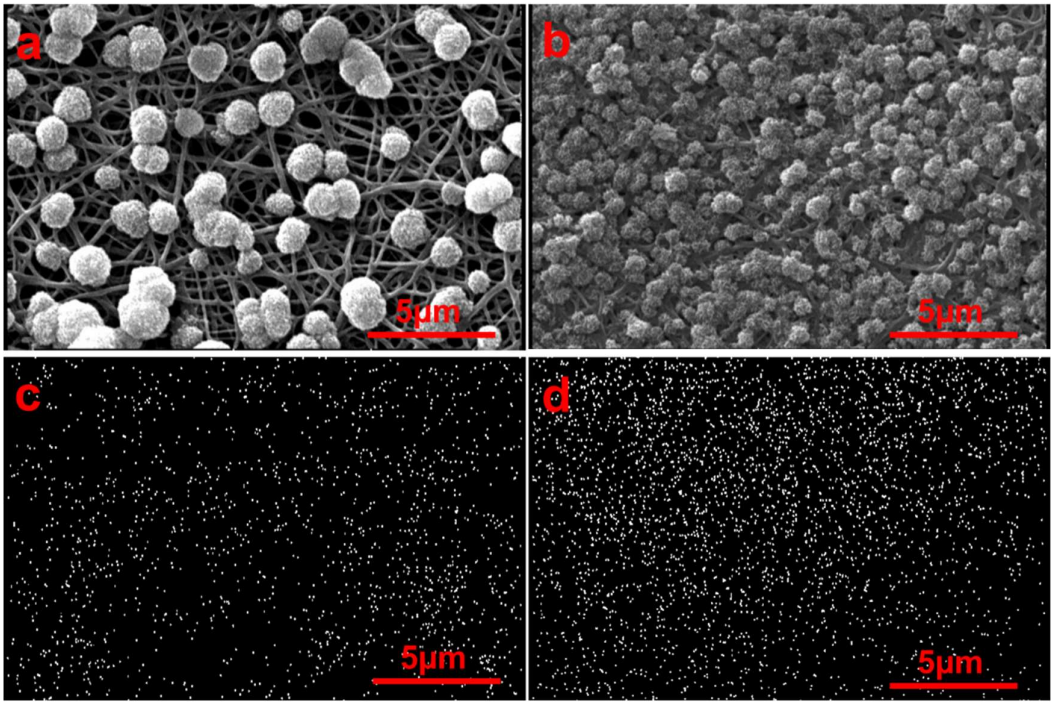

Fig. 3. Osteoactivity of (a) pristine and (b) mineralized CNFs in SBF solution during 14 days.

2.5. Hemocompatibility results

Structures designed to be in contact with blood should be hemocompatible. The hemocompatibility of the prepared nanocomposites was evaluated based on the hemolysis induced by the structures. The results showed that the pristine CNFs induced 12.1 ± 2.1%, which was significantly higher than the negative control group (treated with PBS). On the other hand, the mineralized CNFs induced negligible hemolysis of 5.4 ± 1.8% indicating the nanocomposite's hemocompatibility. The hemolysis of the positive control (blood lysed with DI water) and the negative control (blood treated with PBS) were 100 and 0, respectively.

2.6. Cell attachment and morphology

The morphology of cells on a substrate/scaffold reveals the suitability of the substrate/scaffold for the cell to proliferate and migrate. The morphology of MG-63 cells on the fabricated nanocomposites was observed using SEM after fixation, dehydration and sputter coating with a thin layer of gold, and the results are presented in Fig. 4. The results showed that the cells are

well spread on the mineralized CNFs while holding their partial spherical shape on the pristine CNFs. These observations indicate that the mineralized CNFs favor cells to spread and interact with the scaffold. Yang et al. [30] also reported that osteoblasts MC3T3-E1 cells are well adapted to the mineralized CNFs.

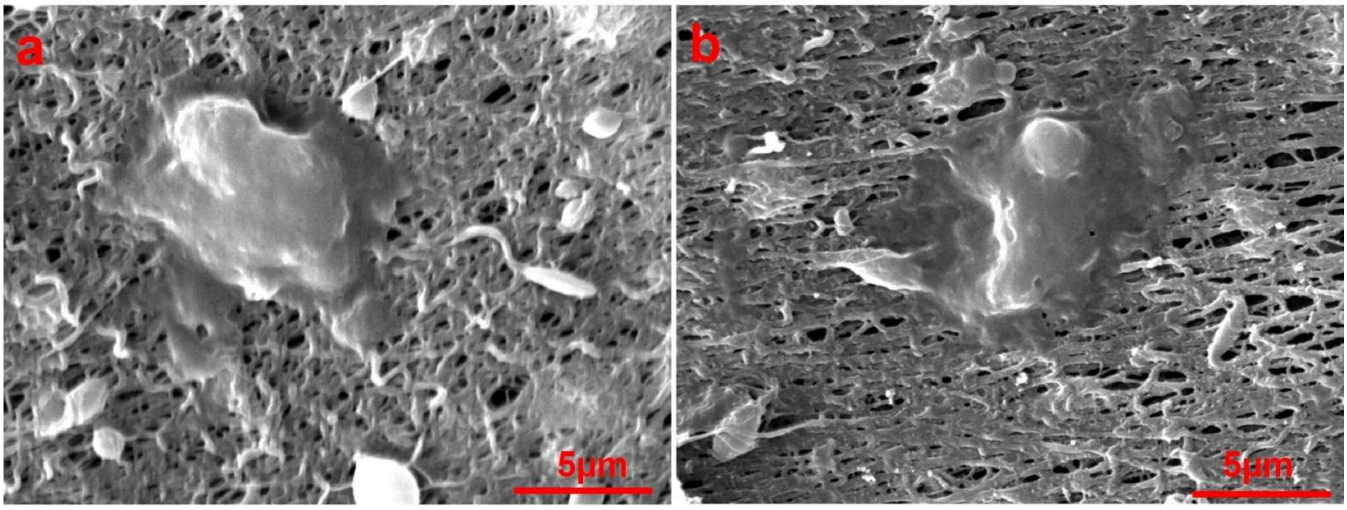

Fig. 4. SEM image of MG-63 cells on (a) pristine and (b) mineralized CNFs

The attachment of MG-63 cells on the nanofibers was also imaged by DAPI staining three days' post-cells seeding. As shown in Fig. 5, the attachment of cells on mineralized CNFs was higher than on pristine CNFs, which can be related to the hydrophilic nature and presence of mineral crystals on the mineralized CNFs.

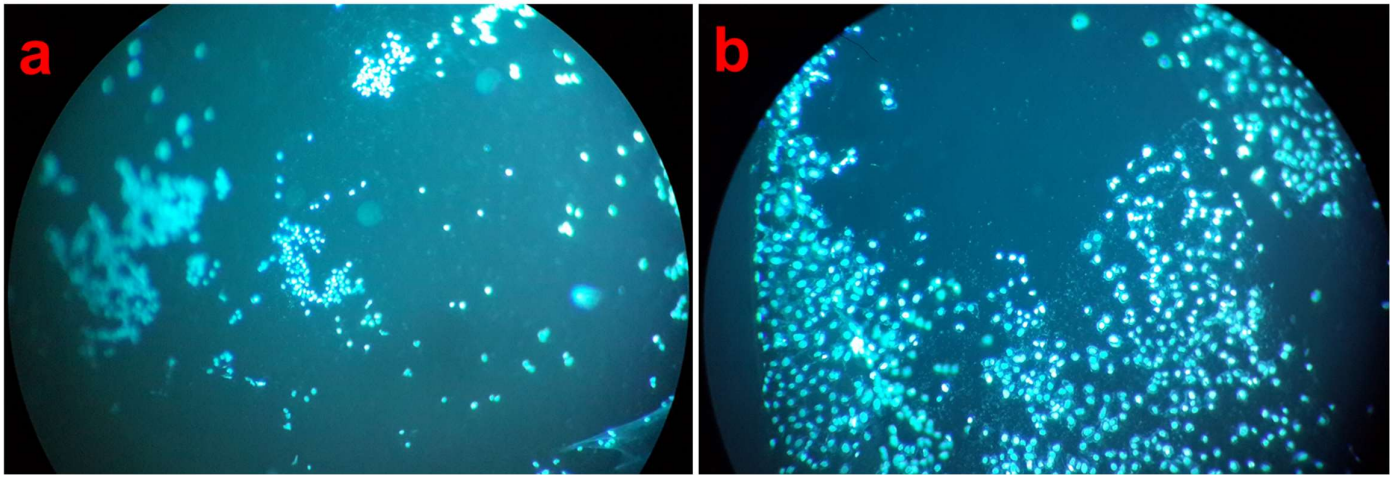

Fig. 5. DAPI staining of MG-63 cells on (a) pristine and (b) mineralized CNFs.

2.7. Cell toxicity results

The MG-63 cell viability/proliferation on the prepared nanofibers was measured quantitatively using the LDH assay kit. The results showed no significant difference in cell viability/proliferation cultured on the control group (tissue culture plastic), pristine CNFs, and mineralized CNFs 24 h after cell seeding. This can be related to the fact that 24 h is a short incubation time for cells to be adapted to the scaffold. The difference between groups was cleared after 72 cell seeding and the viability/proliferation of cells on the mineralized CNFs was significantly higher than control and pristine CNFs ($p < 0.05$). Previous studies showed that pristine CNFs had exhibited some degree of toxicity and the surface treatment increased the biocompatibility [30, 35]. The observed toxicity can be related to the highly hydrophobic surface of CNFs and the absence of cell-beneficial functional groups on pristine CNFs. Accordingly, the surface treatment and inducing proper surface functional groups and elements improve the cytocompatibility of CNFs.

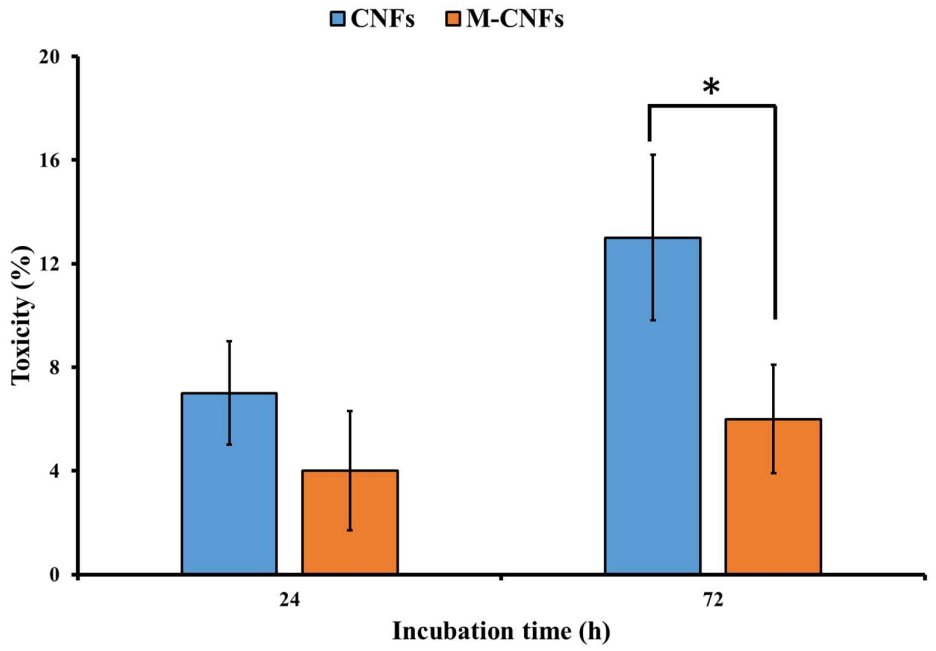

Fig. 6. MG-63 cells toxicity induced by the fabricated CNFs. Values represent the mean ± SD, n: 5, * $p < .05$, (obtained by one-way ANOVA)

3. Conclusion

A practical and sophisticated bone tissue engineering strategy requires scaffolds with the highest architectural and physicochemical similarities to bone native tissues. Accordingly, in the current study, we fabricated electrospun mineralized CNFs composite with excellent electrical conductivity, oesteoactivity, hemocompatibility, and biocompatibility as the bone tissue engineering scaffold. The results indicated that the fabricated nanocomposite supported biomineral deposition, cell attachment, and proliferation. This study revealed that combining the sol-gel method with the electrospun CNFs fabrication method results in mineralized CNFs applicable for bone tissue engineering. The stability, biodegradation, and biopersistence of the implanted biomaterials are critical factors that determine the fate of the biomaterials in the body and efficacy of the treatment strategies. For the future direction, the bone regeneration efficacy

and stability, biodegradation, and biopersistence of the fabricated mineralized nanocomposite should be assessed in animal models.

Conflict of interest:

The authors declare they have no conflict of interest.

Acknowledgment

The authors gratefully acknowledge financial support from the research council of Hamadan University of Medical Sciences (grant no. 140107195951).

References:

[1] A.K. Nair, A. Gautieri, S.-W. Chang, M.J. Buehler, Nature communications 4 (2013) 1.
[2] R. Wang, F. Cui, H. Lu, H. Wen, C. Ma, H. Li, Journal of materials science letters 14 (1995) 490.
[3] H. Samadian, H. Khastar, A. Ehterami, M. Salehi, Scientific reports 11 (2021) 1.
[4] S.S. Jensen, N. Broggini, G. Weibrich, E. Hjôrting-Hansen, R. Schenk, D. Buser, International Journal of Oral & Maxillofacial Implants 20 (2005).
[5] R.R. Betz, Orthopedics 25 (2002) S561.
[6] G.L. Koons, M. Diba, A.G. Mikos, Nature Reviews Materials 5 (2020) 584.
[7] A. Haleem, M. Javaid, R.H. Khan, R. Suman, Journal of clinical orthopaedics and trauma 11 (2020) S118.
[8] A.C. Hernández-González, L. Téllez-Jurado, L.M. Rodríguez-Lorenzo, Carbohydrate polymers 229 (2020) 115514.
[9] Z. Wan, P. Zhang, Y. Liu, L. Lv, Y. Zhou, Acta biomaterialia 101 (2020) 26.
[10] P.N. Christy, S.K. Basha, V.S. Kumari, A. Bashir, M. Maaza, K. Kaviyarasu, M.V. Arasu, N.A. Al-Dhabi, S. Ignacimuthu, Journal of Drug Delivery Science and Technology 55 (2020) 101452.
[11] N. Udomluck, H. Lee, S. Hong, S.-H. Lee, H. Park, Applied Surface Science 520 (2020) 146311.
[12] Q. Zhang, Y. Ji, W. Zheng, M. Yan, D. Wang, M. Li, J. Chen, X. Yan, Q. Zhang, X. Yuan, Journal of Nanomaterials 2020 (2020).
[13] S. Gautam, C. Sharma, S.D. Purohit, H. Singh, A.K. Dinda, P.D. Potdar, C.-F. Chou, N.C. Mishra, Materials Science and Engineering: C 119 (2021) 111588.
[14] Y.P. Singh, S. Dasgupta, S. Nayar, R. Bhaskar, Journal of Biomaterials Science, Polymer Edition 31 (2020) 781.
[15] Z. Li, T. Du, C. Ruan, X. Niu, Bioactive materials 6 (2021) 1491.
[16] H. Liu, M. Lin, X. Liu, Y. Zhang, Y. Luo, Y. Pang, H. Chen, D. Zhu, X. Zhong, S. Ma, Bioactive materials 5 (2020) 844.
[17] L. Leppik, K.M.C. Oliveira, M.B. Bhavsar, J.H. Barker, European Journal of Trauma and Emergency Surgery 46 (2020) 231.
[18] D.M. Ciombor, R.K. Aaron, Foot and ankle clinics 10 (2005) 579.
[19] J.M. Khalifeh, Z. Zohny, M. MacEwan, M. Stephen, W. Johnston, P. Gamble, Y. Zeng, Y. Yan, W.Z. Ray, IEEE reviews in biomedical engineering 11 (2018) 217.
[20] M. Turk, A.M. Deliormanlı, Journal of biomaterials applications 32 (2017) 28.
[21] P. Sikorski, Biomaterials Science 8 (2020) 5583.
[22] H. Derakhshankhah, R. Mohammad-Rezaei, B. Massoumi, M. Abbasian, A. Rezaei, H. Samadian, M. Jaymand, Journal of Materials Science: Materials in Electronics 31 (2020) 10947.
[23] H. Nekounam, S. Gholizadeh, Z. Allahyari, H. Samadian, N. Nazeri, M.A. Shokrgozar, R. Faridi-Majidi, Materials Research Bulletin 134 (2021) 111083.
[24] Z. Peng, T. Zhao, Y. Zhou, S. Li, J. Li, R.M. Leblanc, Advanced healthcare materials 9 (2020) 1901495.
[25] F. Olivier, S. Bonnamy, N. Rochet, C. Drouet, International journal of molecular sciences 22 (2021) 12247.
[26] E. Alimohammadi, A. Nikzad, M. Khedri, M. Rezaian, A.M. Jahromi, N. Rezaei, R. Maleki, Nanomedicine 16 (2020) 189.
[27] A. Bianco, K. Kostarelos, M. Prato, Current opinion in chemical biology 9 (2005) 674.
[28] A. Khoshoei, E. Ghasemy, F. Poustchi, M.-A. Shahbazi, R. Maleki, Pharmaceutical Research 37 (2020) 1.
[29] D. Maiti, X. Tong, X. Mou, K. Yang, Frontiers in pharmacology 9 (2019) 1401.
[30] Q. Yang, G. Sui, Y. Shi, S. Duan, J. Bao, Q. Cai, X. Yang, Carbon 56 (2013) 288.
[31] H. Liu, Q. Cai, P. Lian, Z. Fang, S. Duan, X. Yang, X. Deng, S. Ryu, Materials Letters 64 (2010) 725.
[32] S. Nazarnezhada, G. Abbaszadeh-Goudarzi, H. Samadian, M. Khaksari, J.M. Ghatar, H. Khastar, N. Rezaei, S.R. Mousavi, S. Shirian, M. Salehi, International Journal of Biological Macromolecules 164 (2020) 3323.

[33] H. Nekounam, M.R. Kandi, D. Shaterabadi, H. Samadian, N. Mahmoodi, E. Hasanzadeh, R. Faridi-Majidi, Diamond and Related Materials 115 (2021) 108320.
[34] H. Samadian, H. Mobasheri, S. Hasanpour, R. Faridi-Majid, Journal of Nano Research, Trans Tech Publ, 2017, p. 78-89.
[35] E. Mirzaei, J. Ai, S. Ebrahimi-Barough, J. Verdi, H. Ghanbari, R. Faridi-Majidi, Molecular neurobiology 53 (2016) 4798.
[36] B. Zhang, F. Kang, J.-M. Tarascon, J.-K. Kim, Progress in Materials Science 76 (2016) 319.
[37] J. Jin, B.-j. Yu, Z.-q. Shi, C.-y. Wang, C.-b. Chong, Journal of Power Sources 272 (2014) 800.
[38] Z. Zhou, C. Lai, L. Zhang, Y. Qian, H. Hou, D.H. Reneker, H. Fong, Polymer 50 (2009) 2999.
[39] M. Wu, Q. Wang, X. Liu, H. Liu, Carbon 51 (2013) 335.